FINAL

Direct Retrieval of Line-of-Sight Atmospheric Structure from Limb Sounding Observations

Nathaniel J. Livesey and William G. Read

Jet Propulsion Laboratory, California Institute of Technology, Pasadena, California.

Abstract. Optimal estimation of atmospheric temperature and composition from limb sounding observations is extended to the direct retrieval of line-of-sight atmospheric structure that can be obtained in certain limb viewing geometries. The approach is to divide the dataset into slightly overlapping chunks of several atmospheric profiles and retrieve estimates for all profiles concurrently. The method is made efficient due to the sparse nature of the matrices involved. In the case where the number of radiance measurements is significantly larger than the length of the state vector, the computational effort scales linearly with the number of profiles in the chunk. Prototype simulations, done for the EOS MLS experiment, show that application of this method can give significant improvements in accuracy.

1. Introduction

Limb sounding is a well-established technique for remote sounding of the atmosphere. Past experiments, including the six limb sounding instruments on the Upper Atmosphere Research Satellite (UARS, e.g. *Reber et al.* [1993]) have used both occultation techniques and observations of thermal emission. One of the more complex factors in limb sounding is atmospheric inhomogeneity along the instrument line-of-sight. Previous limb instruments viewed the atmosphere in a direction out of the spacecraft orbital plane. Such a geometry yields little or no direct information on line of sight inhomogeneity, (although a two step retrieve-grid-retrieve process has been implemented in some cases).

The three limb sounding instruments on the CHEM platform (*King* [1999]), scheduled for launch in 2002, represent a new approach to limb sounding, as the instruments' lines-of-sight are generally aligned with the 98° inclined spacecraft orbit plane. The Earth Observing System Microwave Limb Sounder (EOS MLS, see *Waters et al.* [1999]) measures microwave thermal emission in the forward direction. The Tropospheric Emission Sounder (TES) measures thermal infrared emission both in nadir and in backward looking limb geometries. The High Resolution Dynamics Limb Sounder (HIRDLS) measures thermal infrared limb emission at several azimuth angles up to 40° away from the backward direction. These geometries can, if exploited, improve the accuracy of retrieved vertical and horizontal structure.

Figure 1 shows the observation geometry for an instru-

ment such as EOS MLS which makes one complete forward looking limb scan every 1.5° of great circle. The radiances from a single limb scan are affected by the state of the atmosphere over a region spanned by several profiles. For example, the limb ray whose tangent height is 20 km passes through the profiles immediately adjacent to the 'central' profile at an altitude of about 22 km. An appropriately-implemented retrieval algorithm can use this information to more accurately determine the horizontal structure of the atmosphere in the line-of-sight direction.

Figure 1.

2. Theoretical basis

The complete theoretical basis for the EOS MLS retrieval algorithms can be found in the *EOS MLS Retrieval Processes Theoretical Basis Document* (*Livesey and Wu* [1999]). This section briefly outlines the essential details of the algorithm.

2.1. Review of optimal estimation

The use of *optimal estimation* in algorithms for retrieving atmospheric information from remote satellite observations is well established (*Rodgers* [1976, 1990]). While the operational MLS retrieval calculations are non-linear, the innovative approach proposed here can be more simply illustrated by the linear approximation:

$$\mathbf{x} = \mathbf{a} + \left[\mathbf{S}_\mathbf{a}^{-1} + \mathbf{K}^\mathrm{T}\mathbf{S}_\mathbf{y}^{-1}\mathbf{K}\right]^{-1} \mathbf{K}^\mathrm{T}\mathbf{S}_\mathbf{y}^{-1} (\mathbf{y} - \mathbf{f}) . \quad (1)$$

In this equation, $\mathbf{x}$ is the *state vector*, representing the unknown state of the atmosphere for which an estimate is sought. The vector $\mathbf{y}$ with error covariance $\mathbf{S}_\mathbf{y}$ represents the *direct measurements*, such as observed radiances. An initial guess of the state vector is represented by the vector $\mathbf{a}$, typically taken from *a priori* information such as climatology datasets. The vector $\mathbf{f}$ is a set of estimated radiances from a forward model calculation, assuming the atmosphere is in the state represented by $\mathbf{a}$. The matrix $\mathbf{K}$ contains the *weighting functions*. These describe the sensitivity of the radiance observations to the atmospheric state; i.e.

$$\mathbf{K} = \left.\frac{\partial \mathbf{y}}{\partial \mathbf{x}}\right|_{\mathbf{x}=\mathbf{a}} . \quad (2)$$

In this case the vector $\mathbf{a}$, in addition to being used as an initial guess, is also included as a *virtual measurement* of the state vector with covariance $\mathbf{S}_\mathbf{a}$. This is introduced in order to ensure the matrix in equation 1 can be inverted, and to improve knowledge of poorly measured aspects of the system whose eigenvalues are small.

The error covariance of the solution is given by

$$\mathbf{S}_\mathbf{x} = \left[\mathbf{S}_\mathbf{a}^{-1} + \mathbf{K}^\mathrm{T}\mathbf{S}_\mathbf{y}^{-1}\mathbf{K}\right]^{-1} . \quad (3)$$

2.2. Construction of the state vector

The new 'two dimensional' algorithm retrieves geophysical data in 'chunks' of N contiguous geophysical profiles, representing temperature and composition on a fixed set of pressure surfaces, with the forward model assuming linear interpolation between the grid points in the state vector. The state vector is constructed as a set of N subvectors $\mathbf{x}_{[i]}$, each of length n. The measurement vector is similarly constructed from m radiance measurements for each of M separate scans. Typically $N = M$, giving a one to one correspondence between profiles and scans, although more complex distributions of profiles among the scans are possible.

2.3. Matrix aspects of the problem

The $Mm \times Nn$ matrix $\mathbf{K}$ describes the sensitivity of each radiance to elements of the state vector. In this case $\mathbf{K}$ will be sparse, having a 'block band-diagonal' form. For example, the temperature for profile 1 will greatly affect the radiances for the first scan in the chunk, but not the twentieth. The block 'bandwidth' of this matrix is defined as p. Each radiance is affected by $2p + 1$ adjacent profiles. As an example the $\mathbf{K}$ matrix for a simple $N = M = 6$, $p = 1$ case is

$$\mathbf{K} = \begin{bmatrix} \times & \times & 0 & 0 & 0 & 0 \\ \times & \times & \times & 0 & 0 & 0 \\ 0 & \times & \times & \times & 0 & 0 \\ 0 & 0 & \times & \times & \times & 0 \\ 0 & 0 & 0 & \times & \times & \times \\ 0 & 0 & 0 & 0 & \times & \times \end{bmatrix} \tag{4}$$

where 0 indicates an $m \times n$ sub-block of the $\mathbf{K}$ matrix that is identically zero, and $\times$ one that is non zero.

In the EOS MLS case, the matrix $\mathbf{S_y}$ is diagonal, this means that the matrix $\mathbf{K}^T\mathbf{S_y}^{-1}\mathbf{K}$ is also a block band-diagonal matrix with a bandwidth $2p$. In cases such as EOS MLS, where $m \gg n$, the construction of this matrix dominates the computation time in the retrieval. Note that this operation scales linearly in N, making computer memory, not CPU time the limiting factor in setting the value of N. The computation is more time consuming than N separate 1D calculations by a factor of $\sim p$. Yet more efficiency can be gained if the sparsity in the individual submatrices in $\mathbf{K}$ is considered.

The matrix $\mathbf{S_a}$ describes the covariance of the *a priori* information on the state vector. It is useful to describe the *a priori* covariance matrix as a *Kronecker product*

$$\mathbf{S_a} = \mathbf{H} \otimes \mathbf{S_v} \equiv \begin{bmatrix} H_{11}\mathbf{S_v} & H_{12}\mathbf{S_v} & \cdots & H_{1N}\mathbf{S_v} \\ H_{21}\mathbf{S_v} & H_{22}\mathbf{S_v} & \cdots & H_{2N}\mathbf{S_v} \\ \vdots & \vdots & \ddots & \vdots \\ H_{N1}\mathbf{S_v} & H_{N2}\mathbf{S_v} & \cdots & H_{NN}\mathbf{S_v} \end{bmatrix}. \tag{5}$$

The matrix $\mathbf{S_v}$ describes the covariance of a single profile, the matrix $\mathbf{H}$ describes the horizontal correlation between profiles. While this description cannot describe horizontally inhomogeneous uncertainties or height varying horizontal correlations, much efficiency is gained as Kronecker product matrices have the property (*Golub and VanLoan* [1996])

$$\mathbf{S_a^{-1}} = [\mathbf{H} \otimes \mathbf{S_v}]^{-1} = \mathbf{H^{-1}} \otimes \mathbf{S_v^{-1}} \tag{6}$$

2.4. Solving the matrix problem

One manner in which to solve equation 1 is to implement the standard Cholesky decomposition algorithm in a manner which takes advantage of the sparsity of the matrices involved. However, such a method cannot easily take advantage of the Kronecker product structure of $\mathbf{S_a}$. An iterative method can be used to solve the equation by searching for the vector $\mathbf{x}$ that solves

$$\left[\mathbf{S_a^{-1}} + \mathbf{K^T S_y^{-1} K}\right][\mathbf{x} - \mathbf{a}] = \mathbf{K^T S_y^{-1}}\,(\mathbf{y} - \mathbf{f})\,. \tag{7}$$

One such method is the conjugate gradient method (e.g. *Golub and VanLoan* [1996]), whose advantage stems from the fact that the only matrix operation required is matrix-vector multiplication which can be highly optimized for this system. The convergence of the iterative method is greatly improved through the use of a *preconditioner*. The preconditioner is a similar, simpler matrix equation for which solutions are provided each iteration to 'guide' the iterative method more quickly to the solution. One suitable preconditioner is a simpler retrieval of the same dataset, assuming each scan contained information on the 'central' profile alone (the traditional horizontal homogeneity assumption). Using this preconditioner has an additional advantage. By going to the iterative matrix solver, the ability to calculate the solution error covariance of equation 3 is lost. However, this covariance is likely to be well described by the inverse of the preconditioner matrix. This is particularly true of the diagonal elements which are typically all that is reported for the uncertainty on the geophysical products.

2.5. Practical considerations

For numerical reasons the calculations are performed on a set of vectors scaled according to

$$\tilde{\mathbf{y}} = \mathbf{S_y^{-\frac{1}{2}}}\mathbf{y}, \qquad \tilde{\mathbf{x}} = \left[\mathbf{I}_N \otimes \mathbf{S_v^{-\frac{1}{2}}}\right]\mathbf{x}, \tag{8}$$

where $\mathbf{I}_N$ is the $N \times N$ identity matrix. This scaling normalizes the quantities in $\mathbf{x}$ and $\mathbf{y}$ for greater numerical stability, while not breaking the sparsity in $\mathbf{K}$.

Beyond the edges of each chunk, horizontal homogeneity is assumed in both the forward and inverse models. To alleviate the 'edge effects' this introduces, the chunks overlap

by some number of profiles (probably slightly larger than p). While p, the range over which profiles influence radiances, is defined by geometric and radiative transfer considerations, it may be useful to truncate p in some cases for improved efficiency. Choice of such a truncation would be based on careful study of information budgets etc.

In addition to retrieving atmospheric profiles, this scheme can also be used to retrieve 'constant' quantities such as spectroscopic parameters and instrumental calibration. Retrievals based on individual scans typically do not yield enough information on such quantities. However, by retrieving N profiles at a time, useful estimates of them can possibly be obtained. In the operational algorithms N will be about 70, corresponding to data from $\frac{1}{4}$ of a CHEM orbit.

3. Preliminary results

A prototype forward model was constructed which takes into account the two dimensional nature of the problem. In this forward model, p has been limited to 2, thus each scan depends on 5 profiles. The small influence of the more distant profiles has been neglected. The simplified geometry shown in Figure 1 has been assumed. Figures 2 and 3 show some sample weighting functions from this forward model.

Figure 2.

Figure 3.

Observations of optically-thin regions of the atmosphere yield information about constituent concentrations. Observations of optically-thick regions yield 'saturated' radiances which convey information on the temperature of the region of the atmosphere at which saturation occurs. The weighting functions shown below demonstrate the horizontal and vertical properties of this measurement system.

In the case of the O_3 weighting functions, the fact that the atmosphere is optically thin in the given wavelength region leads to a set of weighting functions that are very symmetrical about the center profile. The exception is the left hand profile (closest to the spacecraft) which shows a feature not seen in the last profile (furthest away). This corresponds to the lowest tangent heights, where the atmosphere is optically thick due to the water vapor continuum.

In the case of the temperature weighting functions, the O_2 band is optically thick, and leads to a very asymmetrical set of weighting functions, with the profiles furthest from the spacecraft contributing little or no information to the radiances. The unusual form of the central function is due to the form in which the MLS retrieval and forward model calculations are cast, with geophysical quantities being represented on surfaces of constant pressure. In this coordinate system, the instrument field of view response is, through hydrostatic balance, dependent on temperature. This factor is the dominant term in the derivative of radiance with respect to temperature for the central profile.

This prototype forward model has then been used to com-

pute the terms for a simpler, linear forward model:

$$\mathbf{f} = \mathbf{f}^\star + \mathbf{K}^\star \left[\mathbf{x} - \mathbf{x}^\star\right], \tag{9}$$

where $\mathbf{x}^\star$ is the input state used in the full forward model calculation, and $\mathbf{f}^\star$ and $\mathbf{K}^\star$ are computed radiances and derivatives corresponding to $\mathbf{x}^\star$.

The algorithms described above have been used to retrieve temperature and ozone from simulated radiances in the EOS MLS 118 GHz O_2 and 205 GHz O_3 bands using this linear forward model. 25 profiles of UARS MLS version 5 data for 17 September 1992 have been taken as 'truth', with 'true' radiances computed using the linear model. This dataset corresponds to a series of UARS observations that begin in the strong Antarctic winter polar vortex, cross the vortex edge and finish in mid-latitudes. Note that the horizontal profile spacing for UARS MLS is ~450 km compared to the 165 km for EOS MLS. The structure in our 'true' atmosphere is thus likely to be somewhat severe, but serves as a useful, and probably strongest, test of the algorithm. For comparison, the sharpest temperature gradient in the 'true atmosphere' is $\sim 0.05\,\mathrm{K\,km^{-1}}$, while the sharpest seen in the UARS data for this day is only $\sim 0.03\,\mathrm{K\,km^{-1}}$. The preconditioned conjugate gradient method described earlier was used in the retrieval calculation.

Figure 4.

Figure 5.

The results are given in figures 4 and 5, and show that performing a full 2D retrieval and forward model calculation yields a much more accurate measurement than the simple 1D case. The errors involved in making the 1D approximation are mostly manifested as a lag or a lead in the retrieval relative to the truth. In the case of the temperature retrieval, a lag is seen. This is understandable as the O_2 band is very optically thick. The instrument is obtaining information on the atmosphere closer to the spacecraft than the area to which it is being ascribed in the 1D retrieval. In the ozone case, a lead is observed. This is because the instrument 'sees through' the optically thin atmosphere into the regions of higher ozone concentration, again, the 1D retrieval ascribes this information to the wrong location.

4. Conclusions

It has been shown that direct retrieval of line-of-sight atmospheric structure from limb sounding instruments that view in or near the orbital plane can yield significantly more accurate observations than conventional techniques. This accuracy comes at a relatively low computational cost (typically a factor of $\sim p$, where $2p+1$ is the number of retrieved profiles which affect the radiances obtained on an individual limb scan) compared to the traditional approaches. Results from a simple prototype have shown that this technique leads to more accurate retrieved quantities than previous methods.

Acknowledgments. The authors wish to thank J.W. Waters, M.L. Santee, and the reviewers for useful comments. The research described in this paper was carried out by the Jet Propulsion Laboratory, California Institute of Technology, under a contract with the National Aeronautics and Space Administration.

References

Golub, G., and C. VanLoan, *Matrix Computations, Third edition*, Johns Hopkins University Press, 1996.

King, M., ed., *1999 EOS Reference Handbook*, EOS Project Science Office, Goddard Space Flight Center, 1999.

Livesey, N., and D. Wu, EOS MLS retrieval processes algorithm theoretical basis, *Tech. rep.*, Jet Propulsion Laboratory, 1999, D-16159.

Reber, C., C. Trevathan, R. McNeal, and M. Luther, The Upper Atmosphere Research Satellite (UARS) mission, *J. Geophys. Res.*, *98*, 10,643–10,647, 1993.

Rodgers, C., Retrieval of atmospheric temperature and composition from remote measurements of thermal radiation, *Rev. Geophys.*, *14*, 609–624, 1976.

Rodgers, C., Characterisation and error analysis of profiles retrieved from remote sounding measurements, *J. Geophys. Res.*, *95*, 5,587–5,595, 1990.

Waters, J., et al., The UARS and EOS Microwave Limb Sounder (MLS) experiments, *J. Atmos. Sci.*, *56*, 194–217, 1999.

(Received July 27, 1999; revised November 29, 1999;
accepted not yet.)

LIVESEY AND READ: DIRECT RETRIEVAL OF LINE-OF-SIGHT STRUCTURE

LIVESEY AND READ: DIRECT RETRIEVAL OF LINE-OF-SIGHT STRUCTURE

LIVESEY AND READ: DIRECT RETRIEVAL OF LINE-OF-SIGHT STRUCTURE

LIVESEY AND READ: DIRECT RETRIEVAL OF LINE-OF-SIGHT STRUCTURE

LIVESEY AND READ: DIRECT RETRIEVAL OF LINE-OF-SIGHT STRUCTURE

LIVESEY AND READ: DIRECT RETRIEVAL OF LINE-OF-SIGHT STRUCTURE

LIVESEY AND READ: DIRECT RETRIEVAL OF LINE-OF-SIGHT STRUCTURE

LIVESEY AND READ: DIRECT RETRIEVAL OF LINE-OF-SIGHT STRUCTURE

LIVESEY AND READ: DIRECT RETRIEVAL OF LINE-OF-SIGHT STRUCTURE

LIVESEY AND READ: DIRECT RETRIEVAL OF LINE-OF-SIGHT STRUCTURE

LIVESEY AND READ: DIRECT RETRIEVAL OF LINE-OF-SIGHT STRUCTURE

LIVESEY AND READ: DIRECT RETRIEVAL OF LINE-OF-SIGHT STRUCTURE

Figure Captions

Figure 1. The viewing geometry for a simple model of a forward looking limb sounder such as EOS MLS. The lower plot is an expansion of the boxed region in the upper plot. For each scan, three sets of limb views are shown by the 'horizontal' lines. Horizontal movement of the tangent point is caused by two effects: the motion of the spacecraft, and the decrease in the spacecraft-tangent point distance with increasing tangent point altitude. The vertical scan rate can be chosen to cancel these effects, yielding vertical loci for the tangent points. The retrieved vertical profiles, placed so as to follow these loci, are shown by the black 'vertical' lines. The colored arrows relate the limb radiances to their profiles. (For comparison, the true locus of the tangent points for the case of EOS MLS, including the effects of refraction, is shown for the central profile.)

Figure 1. The viewing geometry for a simple model of a forward looking limb sounder such as EOS MLS. The lower plot is an expansion of the boxed region in the upper plot. For each scan, three sets of limb views are shown by the 'horizontal' lines. Horizontal movement of the tangent point is caused by two effects: the motion of the spacecraft, and the decrease in the spacecraft-tangent point distance with increasing tangent point altitude. The vertical scan rate can be chosen to cancel these effects, yielding vertical loci for the tangent points. The retrieved vertical profiles, placed so as to follow these loci, are shown by the black 'vertical' lines. The colored arrows relate the limb radiances to their profiles. (For comparison, the true locus of the tangent points for the case of EOS MLS, including the effects of refraction, is shown for the central profile.)

Figure 2. Weighting functions describing the sensitivity of radiances from a single channel in the EOS MLS 118 GHz O_2 band to atmospheric temperature. The five plots correspond to the contribution made by five adjacent temperature profiles to a radiance profile whose tangent point locus is co-located with the central temperature profile. The separate lines indicate weightings for different limb tangent heights, the vertical axis describes the pressure within the temperature profiles.

Figure 2. Weighting functions describing the sensitivity of radiances from a single channel in the EOS MLS 118 GHz O_2 band to atmospheric temperature. The five plots correspond to the contribution made by five adjacent temperature profiles to a radiance profile whose tangent point locus is co-located with the central temperature profile. The separate lines indicate weightings for different limb tangent heights, the vertical axis describes the pressure within the temperature profiles.

Figure 3. As Figure 2 except describing the sensitivity of a channel in the 205 GHz band to ozone mixing ratio.

Figure 3. As Figure 2 except describing the sensitivity of a channel in the 205 GHz band to ozone mixing ratio.

Figure 4. Time series of 10 hPa temperature retrieved using prototype algorithms. The solid line indicates truth, the dotted line with + signs indicates results of the full 2D retrieval. The dashed line indicates the results obtained from individual 1D retrievals. The profiles are separated horizontally by 165 km in this simulation.

Figure 4. Time series of 10 hPa temperature retrieved using prototype algorithms. The solid line indicates truth, the dotted line with + signs indicates results of the full 2D retrieval. The dashed line indicates the results obtained from individual 1D retrievals. The profiles are separated horizontally by 165 km in this simulation.

Figure 5. As Figure 4 for 10 hPa ozone.

Figure 5. As Figure 4 for 10 hPa ozone.

Figures

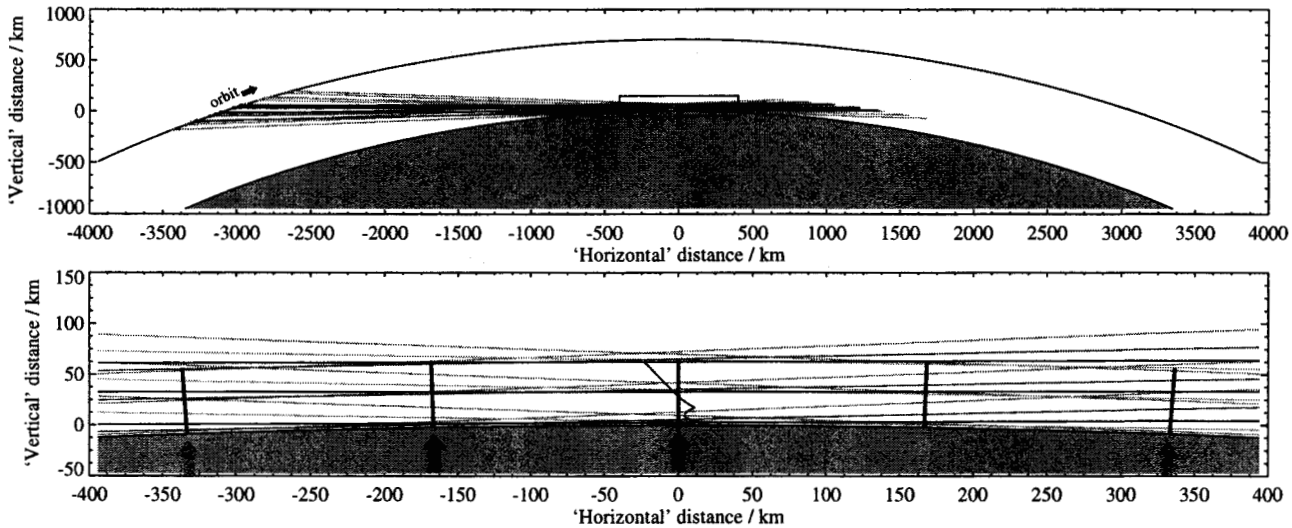

Figure 1. The viewing geometry for a simple model of a forward looking limb sounder such as EOS MLS. The lower plot is an expansion of the boxed region in the upper plot. For each scan, three sets of limb views are shown by the 'horizontal' lines. Horizontal movement of the tangent point is caused by two effects: the motion of the spacecraft, and the decrease in the spacecraft-tangent point distance with increasing tangent point altitude. The vertical scan rate can be chosen to cancel these effects, yielding vertical loci for the tangent points. The retrieved vertical profiles, placed so as to follow these loci, are shown by the black 'vertical' lines. The colored arrows relate the limb radiances to their profiles. (For comparison, the true locus of the tangent points for the case of EOS MLS, including the effects of refraction, is shown for the central profile.)

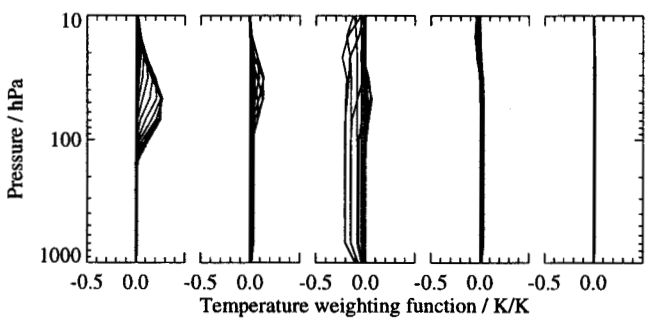

Figure 2. Weighting functions describing the sensitivity of radiances from a single channel in the EOS MLS 118 GHz O_2 band to atmospheric temperature. The five plots correspond to the contribution made by five adjacent temperature profiles to a radiance profile whose tangent point locus is co-located with the central temperature profile. The separate lines indicate weightings for different limb tangent heights, the vertical axis describes the pressure within the temperature profiles.

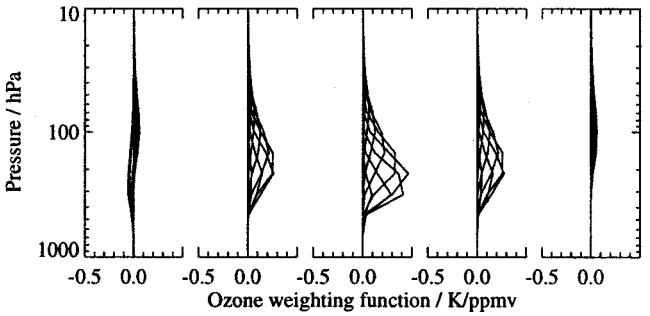

Figure 3. As Figure 2 except describing the sensitivity of a channel in the 205 GHz band to ozone mixing ratio.

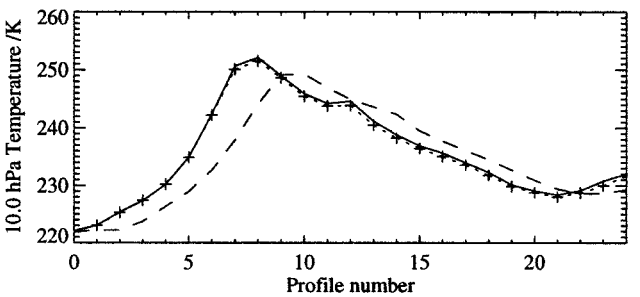

Figure 4. Time series of 10 hPa temperature retrieved using prototype algorithms. The solid line indicates truth, the dotted line with + signs indicates results of the full 2D retrieval. The dashed line indicates the results obtained from individual 1D retrievals. The profiles are separated horizontally by 165 km in this simulation.

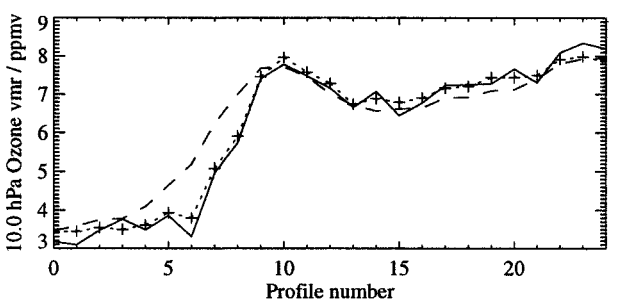

Figure 5. As Figure 4 for 10 hPa ozone.

Paper number

Optimal estimation of atmospheric temperature and composition from limb sounding observations is extended to the direct retrieval of line-of-sight atmospheric structure that can be obtained in certain limb viewing geometries. The approach is to divide the dataset into slightly overlapping chunks of several atmospheric profiles and retrieve estimates for all profiles concurrently. The method is made efficient due to the sparse nature of the matrices involved. In the case where the number of radiance measurements is significantly larger than the length of the state vector, the computational effort scales linearly with the number of profiles in the chunk. Prototype simulations, done for the EOS MLS experiment, show that application of this method can give significant improvements in accuracy.